Available online at www.sciencedirect.com
SCIENCE DIRECT®
Journal of Nuclear Materials 337–339 (2005) 907–911
journal of nuclear materials
www.elsevier.com/locate/jnucmat

Thermal properties of plasma exposed carbon and heat flux calculations on a spatial scale of a few microns

A. Herrmann *

Max-Planck-Institut für Plasmaphysik, EURATOM-IPP Association, Boltzmannstr. 2, D-85748 Garching, Germany

Abstract

Heat flux calculations on the basis of surface temperatures measured thermographically are used at different tokamaks. The spatial resolution of the temperature measurement is in the order of a few millimetres to cope with the expected heat flux gradients. The reliability of the calculated heat flux depends on the degree of agreement between the numerical model and the real situation. This paper discusses effects which alter the measured surface temperature and have to be considered in the heat flux calculation. An inhomogeneous temperature distribution in the field of view of a single detector results in a temperature measuring error which is highest (10%) for a hot component below 50% filling ratio. The limits for the applicability of analytical solutions of the heat flux equation are discussed. Finally, the variation of thermal properties of fine grain graphite and carbon fibre composite on a spatial scale of a few microns, based on experiments presented in [A. Herrmann, M. Bohmeyer, et al., Phys. Scr. T 111 (2004) 98], is presented.

PACS: 67.80.Gb; 68.35.Bs; 44.10.+i; 52.55.Fa
Keywords: Thermography; Materials properties; Thermal conductivity; Carbon-based materials

1. Introduction

Infrared (ir) emission from plasma exposed carbon materials (fine grain graphite (FGG) and carbon fibre composite (CFC)) is used to measure the temperature of in-vessel components in fusion devices. The heat flux is then calculated from the measured temporal evolution of the surface temperature by numerical codes solving the inverse heat conduction problem. The reliability of the resulting heat flux depends on the agreement between the adapted model for heat flux calculation and the real situation. Two main effects have to be considered. (i) The temperature distribution at the surface imaged to a single detector element is not uniform because of heat flux profiles with scale lengths in the order of the pixel image size or from inhomogeneous thermal properties. The measured photon flux is then a mixture of these different temperature components. (ii) The thermal properties of the photon emitting surface are uniform but different from the thermal properties assumed for the calculation. This might be caused by surface modifications due to ion implantation or layer deposition.

How to consider layer effects in the heat flux calculation model depends on the heat capacity of the layer and its thermal contact to the bulk material. A layer with good thermal contact and a stationary temperature distribution can be considered by a heat transmission edge condition, $q_s = \alpha \Delta T$, with the heat transmission coefficient $\alpha = \kappa/d$. The stationary temperature of a layer with

* Tel.: +49 89 3299 1388; fax: +49 89 3299 2580.
E-mail address: albrecht.herrmann@ipp.mpg.de

0022-3115/$ - see front matter © 2004 Elsevier B.V. All rights reserved.
doi:10.1016/j.jnucmat.2004.10.018

bad heat contact is determined by the ratio of heating to radiated power. The heat capacity of the layer affects the temporal evolution of the surface temperature and might introduce a second time scale in the measurement, if the time to establish a stationary temperature profile is long compared to the time between two consecutive measurements. The 2D heat flux code THEODOR [3,4] used for heat flux calculations at ASDEX Upgrade, JET [2] and MAST makes use of such a heat transition edge condition at the plasma facing and the rear side of a thick target.

This edge condition also mitigates effects of an inhomogeneous temperature distribution on a sub-pixel scale which causes an overestimation of the averaged bulk temperature, as will be shown in Section 2, similar to a thin layer on top of the material. The validation of this assumption of a heat transmission edge condition together with the different temporal behaviour of the surface temperature measured in fusion devices on FGG and CFC, was the motivation to investigate the temperature distribution and thermal properties on a few micro meter spatial scale by laser experiments [1,5]. Based on these experiments the consequences of a spatial structure for heat flux calculation and material characterisation are discussed in this paper. The outline is as follows. The error for the temperature measurement due to a spatial variation as input for the heat flux calculation is discussed in Section 2. Section 3 discusses the applicability of simple analytical solutions and consequences for heat flux calculation qualitatively. The application to the measurements is presented in Section 4. Finally, the results are summarized.

2. Temperature error due to a structured target

The typical spatial resolution of ir-systems used at tokamaks is matched to the expected spatial variation of the heat flux in the field of view. Systems with a spatial resolution of a few millimetres are used, e.g. at ASDEX Upgrade [4] and at JET [6] with heat flux e-folding lengths of a few centimeters at the divertor target. In contrast, the spatial structure of the used target material CFC and FGG, respectively, has smaller dimensions than the spatial resolution of the ir-systems, with the consequence that those low resolution systems measure a mixture of photons originating from different temperatures in the field of view of a single pixel (detector element). The resulting spectral distribution is investigated in the near-infrared region [7–9] and correlated with surface layers [10,11]. The temperature derived from the measured photon flux is different from the temperature averaged over the field of view of a single detector, which has to be used for heat flux calculation.

To estimate the resulting error for temperature and heat flux measurements analytically, a two component system is assumed. The photon flux received by the detector is the sum of two contributions, one from the sub-area A_1 at temperature T_h, and the other part from the area $A_0 - A_1$ at temperature T_l. The measured photon flux is then interpreted as originating from a homogeneous temperature [1], resulting in a value for the measured temperature that is not the mean value of the temperature in the field of view (mean temperature). This is shown in Fig. 1 as the temperature error resulting from a difference of the mean temperature of the emitting area ($T_{av} = ((A_0 - A_1) \times T_0 + A_1 \times T_1)/A_0$) and the temperature calculated from the sum of the emitted photon flux for different area ratios ($R_A = A_1/A_0$) and temperature ratios ($R_T = \Delta T_h/\Delta T_l$). It is assumed that both components are in equilibrium below a temperature T_{eq}, the starting temperature of the heating. For all parameter sets the measured temperature is higher than the mean temperature, expressing the strong increase of the photon flux with temperature. The decrease at higher temperatures is due to the smoother change of the photon flux with temperature and consequently a reduced high temperature contribution. The maximum discrepancy is found at an area ratio below 0.5, where the high temperature component contributes less to the mean temperature but a lot of photons to the measured temperature. An area ratio above 0.5 means a dominating contribution of the high temperature component which results in a reduction of the temperature ratio. The error for the worst case (30% of the area is by a factor 2.5 overheated) is below 10% with a maximum near to the start temperature and decreases to a few percent at temperatures above 1000 K. The temperature of the components can be calculated by a one step iteration, if the area and the temperature ratio is known, e.g. from spatially high resolved infrared measurements or from material data.

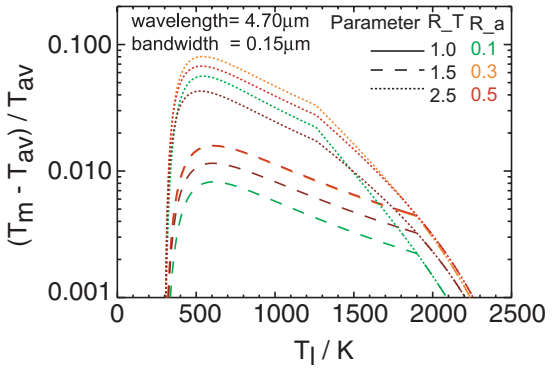

Fig. 1. Error of the measured temperature, T_m, compared to the mean temperature, T_{av}, for a center wavelength of 4.7 µm. The equilibrium temperature is assumed to be $T_{eq} = 300$ K. The error is zero for all R_T and $A_1 = 0$, as well as $R_T = 1$ and all R_A.

3. Heat flux calculation

The geometry and the temperature dependence of the thermal properties of the materials used in fusion devices requires the numerical solution of the heat conduction equation in two or more dimensions. Analytical solutions are available only for special geometries, but they are very useful for a qualitative discussion and they are applicable for quantitative calculations, as long as the restrictions assumed to derive the solution, are considered. In the following, the 1D solution of the heat conduction in semi-infinite slab geometry without source terms and a constant heat flux, q_s, during a time period $0 \leqslant t \leqslant t_1$ is considered. The resulting surface temperature increase for a material with a thermal effusivity $b = \sqrt{\kappa \rho c_p}$ is given by

$$\Delta T_s = \frac{2}{\sqrt{\pi}} \frac{q_s}{b} f(t) \tag{1}$$

with $f(t)$ the time dependence for heating, $\sqrt{t}$, or cooling, $\sqrt{t} - \sqrt{t - t_1}$, respectively. This solution holds also for finite target thickness for times shorter than the heat transfer time, τ_t, through a target of thickness d with a heat diffusivity $a = \kappa/\rho c_p$:

$$\tau_t = \frac{d^2}{8.5a} \tag{2}$$

and for a 2D dimensional surface load, as long as the heat flux into the depth of the material is much larger than the lateral one. The temperature gradient into the depth is given by: $q_s = -\kappa \frac{\partial T_s}{\partial x}$ during the heating phase, whereas the heat flux in y direction can be estimated from the temperature variation along the surface $\partial T_s/\partial y$. A gaussian temperature distribution with standard deviation sigma, σ_y, results in a gradient of $\partial T_s/\partial y = \frac{y}{\sigma_y^2} T_s(y)$. Taking the figures of the laser experiments ($\sigma_y = 1.5$ mm, $T_{max} = 600$ K, $q_s = 70$ MW/m^2, $\kappa = 70$ W/(mK)), the gradient into the depth becomes 1×10^6 K/m and the maximum lateral gradient at $T(\sigma)$, 4×10^5 K/m, which is lower than the gradient into the depth, i.e. the 1D solution of the heat flux equation is applicable for quantitative estimation.

From Eq. (1) it follows that if a structured material with different thermal properties of the components is loaded with a homogeneous heat flux, the resulting temperature pattern at a given point in time during the heat load or the cool down phase (Eq. (1)) reflects the thermal properties of the material if no layer affects the measured surface temperature:

$$b = \frac{2}{\sqrt{\pi}} \frac{q_s}{\Delta T_s} f(t). \tag{3}$$

The separation of heat conductivity and heat capacity is not possible by measuring the surface temperature and using the 1D solution for a semi-infinite target alone. It requires additional information, such as broadening of the profile or some indepth information, e.g. the heat penetration time τ_t (Eq. (2)). The penetration time can be estimated for a thin target from the deviation of the surface temperature from the square-root like time behaviour. The graphite targets used for the laser beam experiments are thick (20 mm) compared to the laser pulse length of 4 ms with a penetration depth of $d_\tau \approx 1.2$ mm.

4. Material parameters on a spatial scale of a few microns

Virgin and plasma exposed CFC as well as virgin FGG was exposed to high heat fluxes from a welding laser with up to 10 J energy per pulse and pulse periods of 10 Hz. The resulting temperature pattern was monitored with a fast 2D ir-camera. Details of the experiment can be found in [1,5]. The measurements are used in the following to derive the heat flux profile of the laser beam, the pattern of the thermal properties and the heat transmission coefficient.

The heat flux profile is deduced from the 2D heat flux calculation, taking into account a heat transmission coefficient at the top. It can be fitted by a gaussian distribution with a standard deviation of 1.6 mm in vertical direction and 1.8 mm in horizontal direction and a maximum heat flux of 70 MW/m^2. The total energy deposited during a single laser pulse to the target as calculated from these profiles is 7 J. This is in good agreement with the laser data of 10 J if a reflectivity of 30% at the carbon surface at a wavelength of 1 μm and transmission losses in the fibre optics are taken into account.

This heat flux distribution is then used to get the normalised thermal property patterns from the temperature distribution during the cool down phase (Eq. (3)), where the heat transmission at the top is negligible (Figs. 2 and 3). The variation of this pattern is about ±10% for FGG and is dominated by normalization and alignment errors rather than by the material properties of FGG. The 2D CFC material with its intrinsic structure show a pronounced thermal property pattern during and immediately after the end of the laser pulse. Later in time, the thermal property pattern is strongly reduced and only a few hot spots remain (Fig. 4, 'isolated' fibre). They are interpreted as fibres with bad heat contact to the surrounding graphite filler as reported from mechanical and thermal loaded CFC ([12,13]). If these hot spots are really carbon fibres it should be concluded, that all the other hot spots are also fibres. The temperature evolution for typical CFC components – fibre, 'isolated' fibre, and filler – are shown in Fig. 4 and compared to FGG. The lowest temperature increase of CFC is comparable to FGG. The temperature decay is faster than for FGG, due to a better heat conductivity in the bulk. This holds even for the 'isolated' fibre. The higher

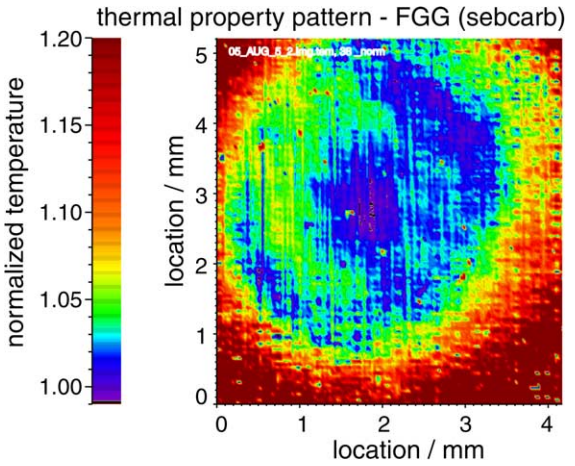

Fig. 2. Pattern of the thermal effusivity of virgin FGG as measured during the cool down phase.

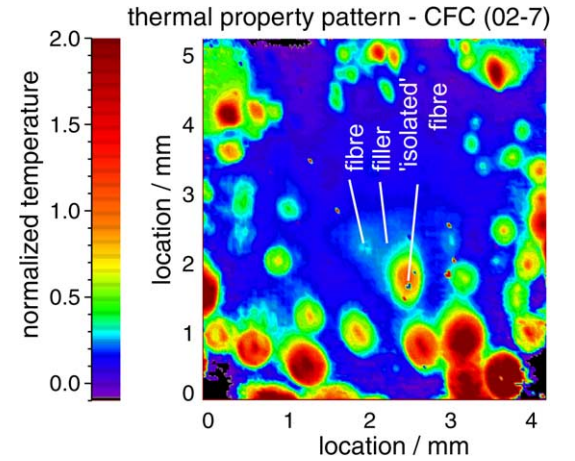

Fig. 3. Pattern of the thermal effusivity of CFC as measured during the cool down phase. The position of the time traces shown in Fig. 4 are marked.

temperature of CFC components might be due to a finite length of the fibre which results in a linear temperature increase for time points longer than the heat penetration time. To be semi-infinite, the fibres should be longer than 1 mm (Eq. (2), $a = 2 \times 10^{-4}\,m^2/s$). The strong increase of the CFC temperature points to damage in the top layer of the CFC material due to the machining rather than to plasma impact, because the virgin CFC shows the same behaviour [1]. This did not alter the macroscopic depth averaged heat conductivity of CFC material as seen from the fast temperature decay (Fig. 4) compared to FGG. The temperature behaviour of the CFC components can not be described by a 1D solution. Nevertheless, the comparison of the expected temperature variation according to Eq. (1) and the

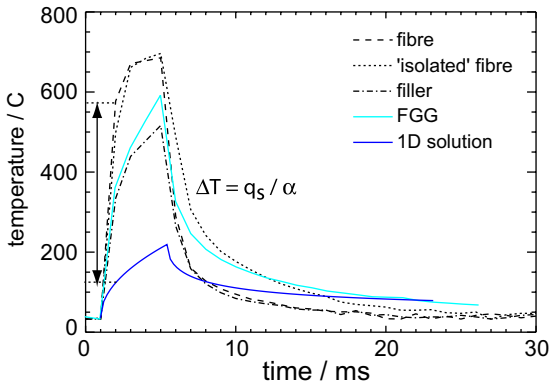

Fig. 4. Temperature evolution for different positions at the CFC target, as marked in Fig. 3, and FGG. For comparision the expected (1D solution) surface temperature evolution for FGG is shown. The strong increase at the beginning of the heating is attributed to a layer described by a heat transmission factor alpha.

measured one show for both materials, FGG and CFC, a layer like behaviour expressed as a temperature jump at the start of the heat pulse (Fig. 4). The heat transmission coefficient deduced from the temperature jump is 300 kW/m^2/K and 150 kW/m^2/K for FGG and CFC respectively. The heat flux was calculated with these input parameters for THEODOR.

5. Summary

Surface effects on thermographic measurements as observed in many tokamaks and in the laboratory results in a measured surface temperature which is higher than the temperature expected from macroscopic material data. These effects are considered by a special heat transmission edge condition in the heat flux code THEODOR. The microscopic structure of the surface temperature pattern is investigated in laboratory experiments. Virgin FGG shows no pronounced structure of the material data, but nonetheless a layer effect which can be modelled by a heat transmission coefficient. The temperature behaviour of CFC is much more complicated and requires a 2D description. In principle, the structure of the material can be parametrized in laboratory experiments or by spectroscopic temperature measurements. The effect of a surface temperature variation on the error of the measured temperature has been estimated by a two component model. It is higher than the mean temperature by up to 10% (Fig. 1). The overestimation of the bulk temperature means that thermography is in a certain sense a 'safe' diagnostic for machine protection, but might reduce the operating range more than necessary.

References

[1] A. Herrmann, M. Balden, W. Bohmeyer, et al., Phys. Scr. T 111 (2004) 98.
[2] P. Andrew, J.P. Coad, Y. Corre, et al., these Proceedings, 2004.
[3] A. Herrmann, ASDEX Upgrade Team, Europhysics Conference Abstracts, in: CD-ROM, Proceedings of the 28th EPS Conference on Controlled Fusion and Plasma Physics, Madeira 2001, p. 2109 (2001).
[4] A. Herrmann, W. Junker, K. Günther, et al., Plasma Phys. Control. Fusion 37 (1995) 17.
[5] D. Hildebrandt, D. Sünder, A. Herrmann, in: Proceedings of Inframation Conference 2003, Las Vegas, USA, 2003.
[6] T. Eich, A. Herrmann, V. Riccardo, et al., Analysis of power deposition in JET MKIIGB by IR-Thermography, in: 28th European Physical Society Conference on Controlled Fusion and Plasma Physics, Funchal, Madeira, 2001.
[7] R. Reichle, V. Basiuk, V. Bergeaud, et al., J. Nucl. Mater. 290 (2001) 701.
[8] E. Delchambre, R. Reichle, R. Mitteau, et al., these Proceedings, 2004.
[9] R. Reichle, C. Brosset, E. Delchambre, et al., these Proceedings, 2004.
[10] R. Reichle, C. Pocheau, E. Delchambre, et al., J. Nucl. Mater. 313 (2003) 711.
[11] E. Delchambre, C. Brosset, R. Reichle, et al., Europhysics Conference Abstracts, in: CD-ROM, Proceedings of the 30th EPS Conference on Controlled Fusion and Plasma Physics, St. Petersburg 2003, (2003).
[12] M. Laux et al., Phys. Scr. T 111 (2004) 184.
[13] S. Pestchanyi, H. Wuerz, Fusion Eng. Des. 66–68 (2003) 271.